J. Fluid Mech. (2014), *vol.* 756, *pp.* 293–308. © Cambridge University Press 2014
doi:10.1017/jfm.2014.456

Resonance patterns in spatially forced Rayleigh–Bénard convection

S. Weiss[1,†], G. Seiden[1,‡] and E. Bodenschatz[1,2]

[1]Max Planck Institute for Dynamics and Self-Organization, D-37073 Göttingen, Germany

[2]Department of Physics, Cornell University, Ithaca, NY 14853-2501, USA

(Received 3 April 2014; revised 27 June 2014; accepted 3 August 2014;
first published online 1 September 2014)

We report on the influence of a quasi-one-dimensional periodic forcing on the pattern selection process in Rayleigh–Bénard convection (RBC). The forcing was introduced by a lithographically fabricated periodic texture on the bottom plate. We study the convection patterns as a function of the Rayleigh number (Ra) and the dimensionless forcing wavenumber (q_f). For small Ra, convection takes the form of straight parallel rolls that are locked to the underlying forcing pattern. With increasing Ra, these rolls give way to more complex patterns, due to a secondary instability. The forcing wavenumber q_f was varied in the experiment over the range of $0.6q_c < q_f < 1.4q_c$, with q_c being the critical wavenumber of the unforced system. We investigate the stability of straight rolls as a function of q_f and report patterns that arise due to a secondary instability.

Key words: Bénard convection, nonlinear dynamical systems, pattern formation

1. Introduction

Many non-equilibrium systems show pattern formation due to spontaneous symmetry breaking when a control parameter exceeds a critical value. Even though the underlying processes can be very different, the patterns that occur and their dynamics are often of striking similarity. Therefore, one can find universal phenomenological equations that describe such systems sufficiently well without considering the details of the elementary processes (Turing 1952; Murray 1989; Cross & Hohenberg 1993; Hoyle 2006; Cross & Greenside 2009). While it is important to study homogeneous isotropic systems to understand the basic mechanisms, patterns in nature are often influenced by parameters and boundary conditions that vary in time and space. Examples of such forced systems include atmospheric convection over topography (Tian, Parker & Kilburn 2003), the formation of fingerprints (Kuecken & Newell 2005), vegetation patterns on hill slopes (Klausmeier 1999), or stone patterns that occur on arctic soils due to frost heave phenomena (Kessler & Werner 2003). These

† Present address: Department of Physics, University of California, Santa Barbara, CA 93106, USA. Email address for correspondence: stwe@umich.edu

‡ Present address: Department of Earth and Planetary Sciences, Faculty of Chemistry, Weizemann Institute of Science, Rehovot, Israel.

https://doi.org/10.1017/jfm.2014.456 Published online by Cambridge University Press

examples are all spatially extended and thus it is important to understand the influence of spatially periodic forcing on the pattern selection.

Rayleigh–Bénard-convection (RBC) is an archetype of pattern forming systems since the underlying mechanisms and the governing equations are well known. Here, a fluid is confined between two horizontal plates held at different temperatures, separated by a distance d from each other. If the bottom plate is warmer than the top plate ($T_b = T_t + \Delta T$) fluid motion occurs when the buoyant force exceeds the damping effects caused by heat and momentum diffusion. The state of the fluid is determined by two dimensionless variables. These are the Rayleigh number:

$$Ra = \frac{\alpha g \Delta T d^3}{\kappa \nu}, \tag{1.1}$$

which represents the ratio between the driving buoyancy and the damping forces, and the Prandtl number:

$$Pr = \frac{\nu}{\kappa}, \tag{1.2}$$

which measures the ratio between thermal and viscous diffusion times. Here α, g, κ, and ν denote the isobaric volume expansion coefficient, the gravitational acceleration, the thermal diffusivity, and the kinematic viscosity, respectively. In a spatially extended isotropic RBC system the conduction state, in which the fluid is at rest, becomes unstable if Ra exceeds the critical value $Ra_c = 1708$. As a result, small fluctuations of the temperature and velocity fields are amplified and fluid motion in the form of parallel rolls sets in. The wavenumber q_c of the fluctuations with the largest growth rate defines the pattern at convection onset. In an isotropic system under Oberbeck–Boussinesq conditions (see e.g. Oberbeck 1879; Boussinesq 1903 and Spiegel & Veronis 1960 for details), the critical wavenumber can be calculated as $q_c = 3.117/d$, corresponding to straight parallel rolls with a periodicity approximately twice the cell height. If Ra is increased above Ra_c, a band of wavenumbers with positive growth rates occurs and convection rolls with these wavenumbers are allowed to exist.

Rolls with a given wavenumber are destabilised by nonlinear interactions whenever Ra exceeds or falls below certain critical values. The region in the Ra–q phase space, in which parallel rolls are stable, i.e. the 'Busse balloon', depends on the Prandtl number (Busse & Whitehead 1971, 1974; Bodenschatz, Pesch & Ahlers 2000). Figure 1 shows the Busse balloon for $Pr = 1.27$, at which experiments presented in this paper were done.

Spatial forcing in the form of light-induced, periodic temperature variations was first used by Whitehead and co-workers (Chen & Whitehead 1968; Busse & Whitehead 1971, 1974) in order to explore the stability region of straight rolls. This enabled them to experimentally confirm theoretically predicted instabilities, such as zigzag, oscillatory (OS) or cross-roll (CR) instability. In addition to the exploration of the stability of convection rolls, spatio-temporal forcing can be utilised in manipulating and controlling pattern forming systems. Applications of such interventions include the suppression of life-threatening cardiac arrhythmias (Luther *et al.* 2011), controlled self-organised nanoparticle devices (Martin *et al.* 2007), or the suppression of ripples occurring on unpaved roads (Taberlet, Morris & McElwaine 2007).

Kelly & Pal (1978) theoretically studied an RBC system where a periodic boundary forcing with wavenumber $q_f \approx q_c$ is applied via (i) flat boundaries with periodic temperature variations and (ii) wavy boundaries with homogeneous temperatures.

https://doi.org/10.1017/jfm.2014.456 Published online by Cambridge University Press

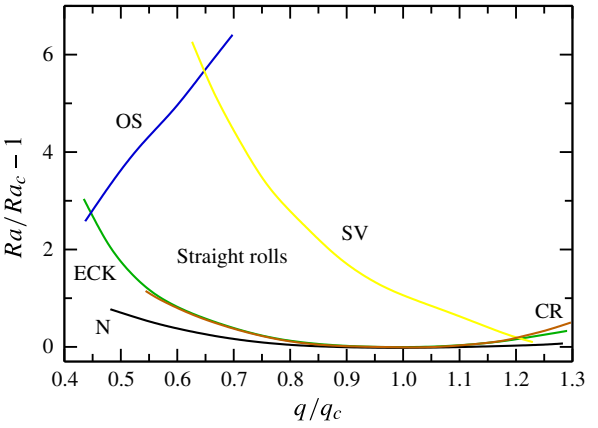


FIGURE 1. (Colour online) Busse balloon for $Pr = 1.27$. The region where straight rolls are stable is confined by a skewed varicose instability (SV), an oscillatory instability (OS), a cross-roll instability (CR), and an Eckhaus instability (ECK). The lowermost line (black online) marks the neutral curve (N).

Focusing on Ra close to Ra_c they found that a pure conduction state is no longer stable and convection sets in gradually for $Ra > 0$. When the forcing parameter δ_f (the relative amplitude of the forcing) is small, the characteristic pitchfork bifurcation at convection onset of the unforced system turns into an imperfect bifurcation in the forced situations.

Spatial forcing has also been used in other pattern forming systems. Lowe, Gollub & Lubensky (1983), Lowe & Gollub (1985), used a periodic array of electrodes in order to study commensurate/incommensurate transitions in nematic liquid crystals. McCoy *et al.* (2008) used a surface modulated bottom plate in a Rayleigh–Bénard set-up to study the influence of periodic forcing with $q_f \approx q_c$ on roll patterns not far from their (unforced) onset Ra_c. They found coherent and localised kink structures that appeared as an instability of straight rolls for sufficiently high control parameters. These kinks showed spatio-temporal chaotic motion. If two kinks met, they either annihilated each other or aggregated to form larger clusters, depending on their orientation. In a similar set-up, in earlier work we have studied the influence of boundary-mediated forcing on an anisotropic pattern forming system (Seiden *et al.* 2008; Weiss, Seiden & Bodenschatz 2012). We used inclined layer convection and changed the relative orientation between the forcing and the anisotropy of the system, i.e. the inclination direction. As a result we discovered a large variety of novel patterns.

Here, we present experiments on forced RBC with varying forcing wavenumbers q_f. The forcing was produced by lithographically fabricated surface texture on the bottom plate. By changing the cell height d we altered the ratio q_f/q_c and explored the instability of straight rolls as the control parameter Ra was increased. We compare our results with the theoretical predictions by Freund, Pesch & Zimmermann (2011), who used a Galerkin method to study this system theoretically. They investigated secondary instabilities of straight rolls that occur as Ra is increased, as a function of the applied forcing wavenumber q_f. Furthermore, they used direct numerical simulation to calculate the patterns that occur as a result of these instabilities.

The paper is organised as follows. The next section will give a brief overview of the experimental set-up. In § 3 we will show the stability region and discuss in

https://doi.org/10.1017/jfm.2014.456 Published online by Cambridge University Press

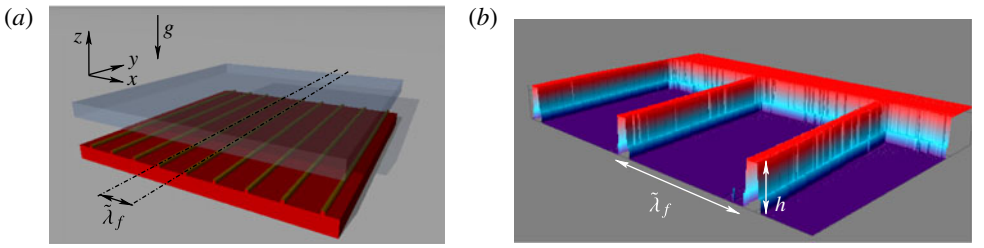


FIGURE 2. (Colour online) (*a*) Sketch of the convection cell with surface modulation of the bottom plate. (*b*) Profile of the bottom plate texture as measured by white-light interferometry.

detail patterns that occur when straight rolls become unstable upon increasing *Ra*. We conclude with a short summary.

2. Experimental set-up

Our convection apparatus is similar to the one described by de Bruyn *et al.* (1996). Since a detailed description can be found in Plapp (1997) we only give a brief summary here. We used compressed CO_2 at a pressure of 50 bar as a working fluid. This enables the investigation of large-aspect-ratio convection cells with sufficiently short diffusion time scales to observe non-transient states. A typical vertical viscous diffusion time $\tau_v = d^2/\nu$ was of the order of three seconds. The gas was confined by a 9.5 mm thick single crystalline silicon plate from below and a similar sapphire plate from above. Using interferometry we adjusted both plates to be parallel within 1 μm. The temperatures of the top (T_t) and the bottom (T_b) plates were held constant to within 1 mK during the experiment. The average temperature used in the experiments presented here was $T_{av} = (T_b + T_t)/2 = (27 \pm 0.001)\,^{\circ}\mathrm{C}$ resulting in $Pr = 1.27$.

The sidewalls of our convection cells were made out of slips of paper to match the thermal properties of the gas and thus minimise the influence of the lateral boundaries. Convection took place in two square cells with side lengths $L = 46$ and 19 mm. While the larger cell had a modulated bottom plate surface, the smaller one served as an unforced reference cell. The large cell was aligned with its lateral boundaries parallel to the forcing structure in order to minimise perturbations of forced straight rolls due to the sidewall (Bodenschatz *et al.* 2000, and references therein).

Forcing was applied by texturing the bottom plate via photo lithography. The texture consisted of long polymer ridges (SU-8) of height $h = (65 \pm 3)$ μm, width $l = 100$ μm and periodicity of $\tilde{\lambda}_f = 1$ mm, covering the whole area of the larger cell (figure 2). Note, that we use $\tilde{\lambda}_f$ to denote the forcing wavelength in physical units, whereas we write the dimensionless forcing wavelength as $\lambda_f = \tilde{\lambda}_f/d$.

The quasi-one-dimensional forcing we applied introduces, to first order, two independent forcing parameters. The first is the forcing wavenumber $q_f = 2\pi/\lambda_f$ and the second the forcing strength. The latter can be written as $\delta_f = a_1 h/d$, where a_1 denotes the first Fourier coefficient of the Fourier approximation of the surface profile, and has a value of $a_1 = 0.196$. In the dimensionless Boussinesq equations, which describes RBC dynamics, lengths are expressed in units of d. Therefore, we changed q_f in the experiment by varying d while keeping the texture, i.e. $\tilde{\lambda}_f$, unchanged. While this saved us from manufacturing a new bottom plate for each experimental run, this procedure has two disadvantages. First, whenever we change

https://doi.org/10.1017/jfm.2014.456 Published online by Cambridge University Press

q_f we also change the forcing strength δ_f proportional to $1/q_f$. Secondly, by reducing the cell height one needs to increase the temperature difference ΔT in order to achieve the same *Ra*. If ΔT becomes too large, the fluid becomes more and more non-Boussinesq and fluid parameters vary between top and bottom plate (Busse 1967; Tschammer 1996).

Imaging the convection flow was done by using the shadowgraph technique (Rasenat *et al.* 1988; Berry & Bodenschatz 1999; Trainoff & Cannell 2002) in combination with a CCD camera as described in de Bruyn *et al.* (1996). By means of light focusing, cold regions where the fluid flows towards the bottom plate are imaged as bright areas, whereas warm up-flow regions are imaged as darker areas. All images were divided by a reference image that was taken at $\Delta T = 0$ K in order to reduce light inhomogeneities across the sample.

As described by Plapp (1997) the cell height d could easily be changed by adjustment screws from outside the apparatus. While in this way we could change d by a few tens of μm, for larger changes the height of the lateral sidewall also had to be changed and thus the apparatus had to be opened. During a typical experimental run the cell height was first determined by measuring the convection onset in the unforced reference cell via $d = (1708\nu\kappa/\alpha g\Delta T_c)^{1/3}$. Then, the temperature difference ΔT was raised in small steps. After each raise, the system was given sufficient time to equilibrate to a non-transient state ($\approx 100\tau_v$), before pictures were taken of the observed pattern.

3. Results

3.1. *The phase diagram*

As discussed elsewhere (e.g. Kelly & Pal 1978; Seiden *et al.* 2008: Freund *et al.* 2011) under quasi-one-dimensional periodic forcing a pure conduction state cannot exist for any positive *Ra*. Instead, the system develops straight parallel rolls, that are in phase with the underlying forcing pattern. In the case of resonant forcing ($q_f = q_c$), the amplitude of the rolls increases with increasing ε following an imperfect bifurcation.

In the following we use the normalised temperature difference as the control parameter $\varepsilon \equiv \Delta T/\Delta T_c - 1$, with ΔT_c being the critical temperature difference for which the onset of convection was observed in the unforced reference cell. Note that this definition is equivalent to $\varepsilon \equiv Ra/1708 - 1$.

Figure 3 shows the parameter space investigated, that is spanned by ε and the normalised forcing wavenumber q_f/q_c. The upper x-axis shows the corresponding δ_f. Experiments were conducted in the range of $0.63 \leqslant q_f/q_c \leqslant 1.4$. Each symbol marks a distinct pattern that was observed in the experiment. The bullets mark straight rolls, that are phase locked with the underlying forcing structure (see also figure 4*a*). The rolls are the dominant pattern for $\varepsilon < 0$ but become unstable when ε exceeds certain critical values ε_c that depend on the applied forcing wavenumber q_f/q_c.

For $q_f/q_c < 0.75$, theory predicts two regions of stability for straight rolls (dashed line in figure 3). Straight rolls lose stability at about $\varepsilon_c \approx 0$, but regain stability at larger ε. We observed the lower instability line, for three different q_f, but we could only measure the upper instability line for $q_f = 0.74q_c$, due to experimental constraints. For slightly larger q_f/q_c, straight rolls are stable and ε_c is rather large, but decreases with increasing q_f/q_c. Due to experimental limitations (Oberbeck–Boussinesq conditions), the stability boundary of straight rolls could not be reached in the range $0.75 < q_f/q_c < 1$. Nevertheless, we can state that ε_c does not have its maximum at $q_f/q_c = 1$ as one would naively expect, but rather at smaller forcing

https://doi.org/10.1017/jfm.2014.456 Published online by Cambridge University Press

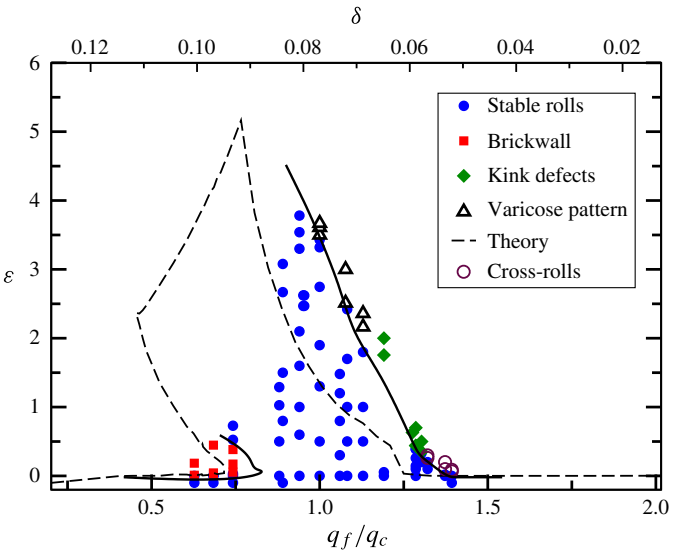


FIGURE 3. (Colour online) Stability region of straight forced rolls with wavevector q_f and their instability line. Symbols mark parameters where the patterns listed in the figure legend were observed. The solid lines are hand drawn instability boundaries as a guide to the eye. Dashed lines are the theoretically calculated instability line of straight rolls, as calculated by Freund *et al.* (2011).

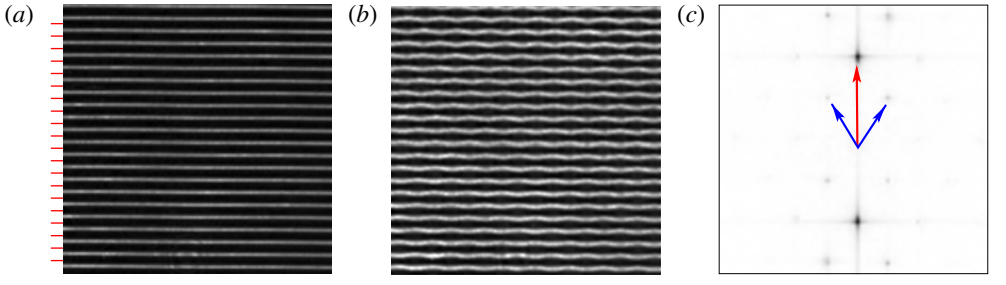


FIGURE 4. (Colour online) (*a*) Straight parallel rolls with wavenumber q_f appear in the forced cell for $\varepsilon = 2.13$. (*b*) VP at $\varepsilon = 2.76$. (*c*) Fourier transform of (*b*): the vertical arrow (red online) marks the forcing mode $\boldsymbol{q}_f$ and the angled arrows (blue online) mark the two phase-modulating modes $\boldsymbol{q}_1$ and $\boldsymbol{q}_2$. Patterns shown here were observed in experiments with $q_f/q_c = 1.08$.

wavenumbers, as suggested by Freund *et al.* (2011). This can be understood, since the stability region of straight rolls resembles the overall shape of the Busse balloon of the unforced system (figure 1), which clearly leans towards smaller wavenumbers. For $1 \lesssim q_f/q_c < 1.4$ the stability line of forced rolls decreases with increasing q_f/q_c and reaches $\varepsilon_c = 0$ for $q_f/q_c = 1.4$.

As a result of the instability of straight rolls, new patterns arise. These patterns are varicose patterns (VP) for $1 \lesssim q_f/q_c \lesssim 1.13$, coherent kink lines and localised kink defects for $1.19 \lesssim q_f/q_c \lesssim 1.30$, and cross-rolls (CR) for $1.32 \lesssim q_f/q_c < 1.39$. Furthermore, we found a brickwall pattern (BW) for $q_f/q_c < 0.75$. For $q_f/q_c = 0.75$ BW disappeared when ε was raised above 0.5 and straight rolls became stable again.

https://doi.org/10.1017/jfm.2014.456 Published online by Cambridge University Press

We note that in the latter range, the cell height was rather small. Therefore the forcing strength δ_f and ΔT were large, both effects leading to a broken up/down symmetry between cold and warm areas (i.e. non-Boussinesq effect). As we will see below, BW consist of three wavevectors, that build a resonant triad, which is typical for patterns occurring in systems with a broken up-down symmetry (see for example Cross & Hohenberg 1993; Rogers *et al.* 2000; Porter & Silber 2004).

The dashed line in figure 3 represents the numerically calculated instability boundaries of straight rolls. We used the Galerkin code that was developed by W. Pesch and coworkers (Freund *et al.* 2011) to test the stability of straight rolls with respect to periodic perturbations with wavevector $\boldsymbol{s}$ (Floquet vector). It should be noted that this is different from the rectangular-profile periodic ridges used in our experiments. As mentioned earlier, a detailed description of the theoretical model and the Galerkin method was previously published by Freund *et al.* (2011). In this theoretical description, the modulated bottom plate surface was treated as a sinusoidal modulation of the bottom plate temperature. Their calculations were done with $Pr = 1$ and different values of δ_f that were however each held constant while q_f/q_c was changed. We recalculated the stability regions for $Pr = 1.27$ to better compare with the experimental results. In addition, we also took into consideration that δ_f decreases as q_f/q_c increases and adopted δ_f for each q_f/q_c accordingly.

As can be seen in figure 3, the experimental points that correspond to stable straight rolls agree qualitatively with the theoretical prediction, but disagree quantitatively. In accordance with theory, there are two ranges at very small and rather large q_f/q_c where straight rolls become unstable close to $\varepsilon = 0$. Furthermore, the large values of ε_c close to $q_f/q_c \approx 1$ are predicted correctly. Theory also predicts the strongly overhang of the stability region on the left, where rolls become unstable at $\varepsilon \approx 0$, but become stable again for some larger values $\varepsilon > \varepsilon_{c2}$. Due to experimental limitation we only have a single value of $q_f/q_c = 0.74$, which, however, agrees with that prediction.

Discrepancy with the theory is found when comparing quantitatively the exact locations of the stability boundaries. The boundaries predicted by theory (dashed curve in figure 3) do not overlap with the experimental observations (solid line in figure 3). In the range $1 < q_f/q_c < 1.3$, the instability of rolls appears in the experiment at noticeably larger values of ε compared to the theory. On the other side, for $q_f/q_c \leqslant 0.75$ the tip of the wedge of the straight-roll region is predicted at $q_f/q_c \approx 0.72$, whereas the experimental result is $q_f/q_c > 0.75$. The origin of the discrepancy lies most likely in the theoretical assumptions regarding the form of the periodic forcing applied to the boundary. A more detailed discussion is deferred to § 4.

In the following subsections, we will have a closer look at the observed instabilities and the patterns emerging when straight rolls become unstable.

3.2. *Near-resonant forcing* ($q_f \approx q_c$)

When the forcing wavenumber was close to the critical wavenumber of the unforced system, straight rolls were stable up to a relatively high ε (figure 3). At the stability boundary, straight rolls turn into a varicose pattern (VP) (open black triangles in figure 3). Figures 4(*b*) and 4(*c*) show a shadowgraph image of VP and a corresponding Fourier transform. VP are characterised by a periodic phase modulation of the original straight rolls. Next to the forcing mode $\boldsymbol{q}_f = (0, q_f)$ two side modes appear in the Fourier spectrum:

$$\boldsymbol{q}_1 = q_f\,(q_x, 0.5) \quad \text{and} \quad \boldsymbol{q}_2 = q_f\,(-q_x, 0.5). \tag{3.1a,b}$$

https://doi.org/10.1017/jfm.2014.456 Published online by Cambridge University Press

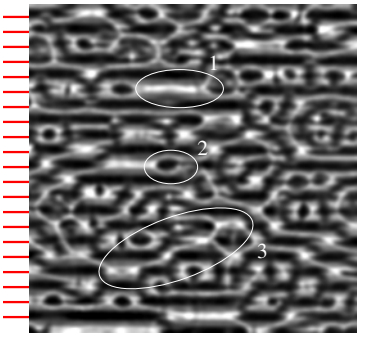


FIGURE 5. (Colour online) Spatio-temporal chaos at $q_f/q_c = 1.08$ and $\varepsilon = 2.79$. The lines at the left mark the locations of the SU-8 ridges. These patterns consist of several localised structures such as short subharmonic rolls (1), small ringlet structures (2) and kink defects (3).

Here, q_x does not change with ε, but depends on the forcing wavenumber q_f/q_c. With increasing q_f/q_c, q_x increases from $q_x = 0.33$ at $q_f/q_c = 1.01$ to $q_x = 0.37$ at $q_f/q_c = 1.13$. VP are steady in time. VP were also observed in forced inclined layer convection, when the in-plane gravity component was parallel to the forcing texture (Seiden *et al.* 2008; Weiss *et al.* 2012).

If one increases ε, the amplitude of the phase modulation of VP increases until two adjacent rolls merge, creating a defect. The whole pattern then turns abruptly into a spatio-temporal chaotic state as shown in figure 5. This state consists of many different localised structures, that exhibit chaotic dynamics. While small areas are covered with short straight rolls with wavelength $3\lambda_f/2$ (with $\lambda_f = 2\pi/q_f$, encircled region 1 in figure 5) at other places, localised kink defects (region 3 in figure 5) and ringlets (region 2 in figure 5) exist. We note that in simulations of the full Boussinesq equations Freund *et al.* (2011) found a transition from straight rolls to a spiral defect chaos (SDC) state. In contrast to SDC observed in unforced convection, there the patterns are anisotropic with rolls having a general tendency to align along the forcing direction. Features like ringlets and kinks appear in the simulation that are similar to the ones observed in our experiment.

Note that the VP are bistable and can only exist if ε is increased slowly after the system had developed straight parallel rolls. If instead ε is decreased from a chaotic state similar to the one shown in figure 5, the system changes continuously from that state to straight rolls, by decreasing the number of defects. In this regime, we could observe a state of localised kink defects that interact with each other and, depending on their orientation, are either annihilated or clustered together to form kink crystals as reported previously by McCoy *et al.* (2008).

3.3. *Kink patterns*

In the range $1.12 \lesssim q_f/q_c \lesssim 1.3$ the upper boundary of straight rolls still occurs at rather large ε, but is observed to strongly decrease with increasing q_f/q_c (figure 3). If ε exceeds the stability line, coherent kinks form (diamonds in figure 3). These are localised phase defects that arrange themselves into lines that are inclined with an angle α to the SU-8 ridges (figure 6). Kinks have already been investigated by McCoy (2007) and McCoy *et al.* (2008) in a very similar experiment with $q_f/q_c = 1.2$.

https://doi.org/10.1017/jfm.2014.456 Published online by Cambridge University Press

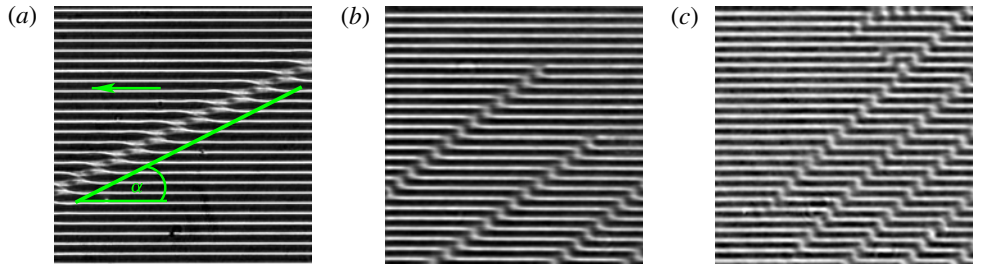


FIGURE 6. (Colour online) Coherent kink lines for different forcing wavenumbers: (*a*) $q_f/q_c = 1.191$, (*b*) $q_f/q_c = 1.276$ and (*c*) $q_f/q_c = 1.321$. The arrow in (*a*) marks the direction of motion of the kink line.

In contrast to our experiment, their cell had a circular shape which influences the system, since often kinks nucleate at the lateral boundary. Furthermore, kinks were also observed in forced inclined layer convection by Seiden *et al.* (2008) and Weiss *et al.* (2012), where they also formed coherent lines like in the horizontal case which slowly drifted in the downhill direction.

One qualitative feature of the coherent kink lines is the angle α that these lines make with the underlying forcing pattern. This angle depends on the forcing wavenumber and becomes slightly larger when q_f/q_c is increased: $\alpha = 27^\circ$ at $q_f/q_c = 1.19$ (figure 6*a*) and $\alpha = 47^\circ$ at $q_f/q_c = 1.30$ (figure 6*c*). Coherent kink lines drift slowly along the forcing structure as marked by an arrow in figure 6(*a*).

VP and kinks are most likely of the same origin for the following reasons. First, in the q_f/q_c-range where VP exist, kinks are found when ε is decreased slowly out of a spatio-temporal chaotic state. Secondly, in the q_f/q_c-range where kinks exist, VP were observed as a transient state when ε was increased sufficiently fast (McCoy 2007). In this context, note also that kinks and VP coexist next to each other in forced inclined layer convection (Seiden *et al.* 2008; Weiss 2009; Weiss *et al.* 2012). And thirdly, in theoretical considerations the right-hand side of the wedge-shaped stability region of straight rolls is only confined by a single instability (a skewed varicose, SV, instability) instead of two different ones, as found here (Freund *et al.* 2011).

3.4. *Cross-roll (CR) patterns*

At $q_f/q_c > 1.32$ forced rolls become unstable at $\varepsilon \approx 0$ to a cross-roll pattern (figure 7*a*). Forced rolls with $\boldsymbol{q}_f$ are superimposed by rolls perpendicular to them with wavevector $\boldsymbol{q}_1 = (q_c, 0)$ (figure 7*b*). This instability is comparable to the cross-roll instability (Busse 1978; Bodenschatz *et al.* 2000) that occurs in fluids with large Prandtl numbers on the right-hand side of the (unforced) Busse balloon. In the unforced case, an existing roll pattern with wavenumber $q > q_c$ is replaced by convection rolls with a smaller wavenumber that are aligned perpendicular to the original rolls. This instability mechanism occurs for large Pr and is replaced by the Eckhaus instability for low-Prandtl-number fluids. A CR instability also appears as a mechanism to increase the wavenumber of rolls, when $q < q_c$. However, in these latter cases the instability appears only locally and produces a dislocation that moves and thus increases the wavenumber of the system.

The CR instability shown in figure 7 is different to what is predicted by theory (Freund *et al.* 2011). Both a Galerkin analysis and direct numerical simulations (DNS)

https://doi.org/10.1017/jfm.2014.456 Published online by Cambridge University Press

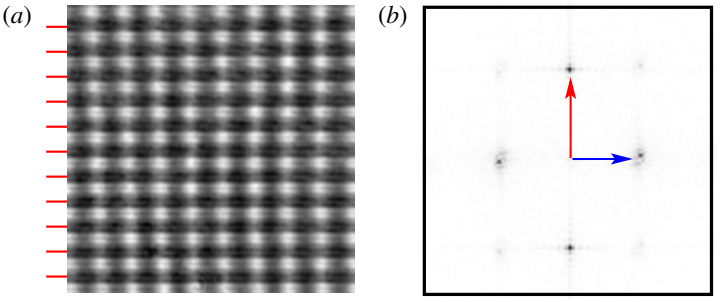


FIGURE 7. (Colour online) (*a*) Cross-roll pattern taken at $q_f/q_c = 1.39$ and $\varepsilon = 0.21$. The lines at the left mark the forcing structure. (*b*) Its Fourier transform: the vertical arrow (red online) marks $\boldsymbol{q}_f$, and the horizontal arrow (blue online) marks $\boldsymbol{q}_1$.

show in this q_f/q_c-range that straight rolls become unstable first to two modes $\boldsymbol{q}_1$ and $\boldsymbol{q}_2$ with moduli $q_1 = q_2 = q_c$ that resonate with $\boldsymbol{q}_f (\boldsymbol{q}_f = \boldsymbol{q}_1 + \boldsymbol{q}_2)$. As a result a rectangular pattern occurs. For slightly larger ε, theory predicts that the amplitude of one of these modes dominates the other and an oblique roll pattern emerges. The same behaviour was also found in simulations of the parametrically forced Swift–Hohenberg equation by Manor, Hagberg & Meron (2008) and Mau *et al.* (2013). Possible reasons for the discrepancy will be discussed in § 4.

With increasing ε, the amplitude of $\boldsymbol{q}_1$ increases, relative to that of $\boldsymbol{q}_f$. The bimodal pattern turns continuously into a roll pattern with wavenumber q_c, whose intensity is modulated by the bottom plate texture. These rolls behave similarly to the unforced rolls in the reference cell. They start to bend towards the sidewalls and reach a state of spatio-temporal chaos as ε is further increased. In this more chaotic state one finds kink defects and subharmonic resonances. This transition from CR to a spatio-temporal chaotic state is shown in detail in figure 8. At $\varepsilon = 0.14$ the pattern has already turned continuously into rolls that are not perpendicular to the forcing texture but tend to bend to the sidewall. At $\varepsilon = 0.33$ in some areas (lower left corner) a kink structure appears while in large parts of the cell rolls exist that are modulated by the underlying forcing structure. The kink structure becomes more pronounced at $\varepsilon = 0.41$ and at $\varepsilon = 0.60$ areas with subharmonic resonances occur. For even higher ε the pattern becomes spatio-temporal chaotic and consists of targets, spirals and subharmonic resonances.

3.5. *Brickwall (BW) pattern*

As mentioned above, the relative forcing wavelength q_f/q_c was changed by changing the cell height. For resonant forcing ($q_f/q_c \approx 1$) and for forcing with slightly lower q_f, forced rolls are stable and their instability line is shifted to very large ε. Furthermore, to reach a certain value of ε, ΔT increases with decreasing q_f/q_c (since ΔT_c increases with decreasing d). Therefore, the maximal ε that could be achieved in the experiment decreased constantly with decreasing q_f/q_c. As a result, it was not possible to reach the instability line of the forced rolls in the range $0.75 < q_f/q_c < 0.95$.

For $q_f/q_c < 0.75$, forced straight rolls become unstable at $\varepsilon \approx 0$ with respect to two symmetric wavevectors $\boldsymbol{q}_{1,2} \approx q_f(\pm q_x, 0.5)$, that produce together with $\boldsymbol{q}_f$ a brickwall pattern (figure 9). The exact value of q_x decreases with increasing ε. As an example, for $q_f/q_c = 0.68$, it is at instability onset ($\varepsilon = 0.03$), $q_x \approx 1.4$ whereas for $\varepsilon = 0.46$ it is $q_x \approx 1.23$.

https://doi.org/10.1017/jfm.2014.456 Published online by Cambridge University Press

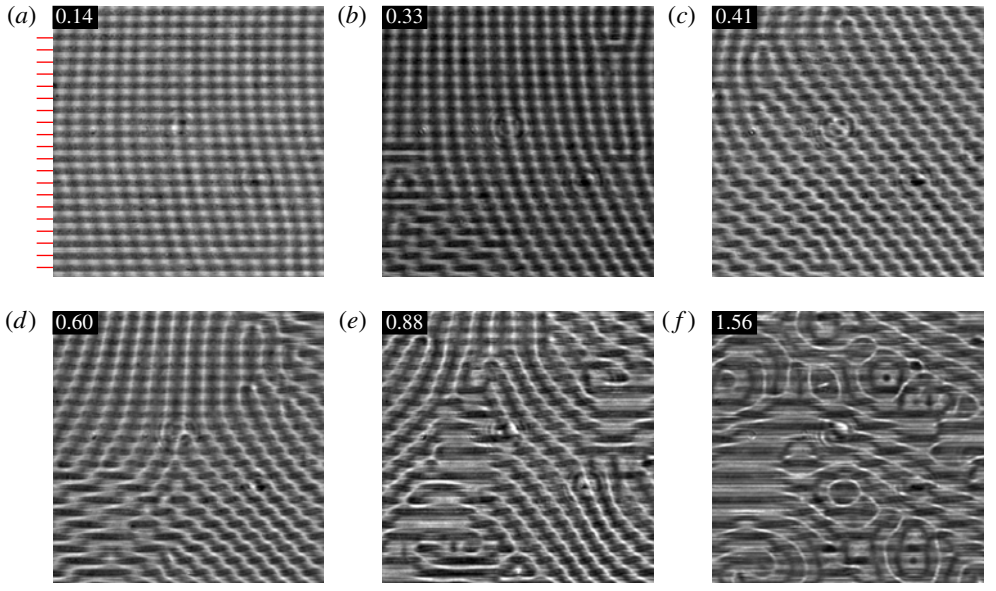


FIGURE 8. (Colour online) Cross-roll pattern and its transition to a spatio-temporal chaotic state. The images were taken at $q_f/q_c = 1.39$ and various ε as marked on each image. The lines at the left of the first image mark the location of the SU-8 ridges.

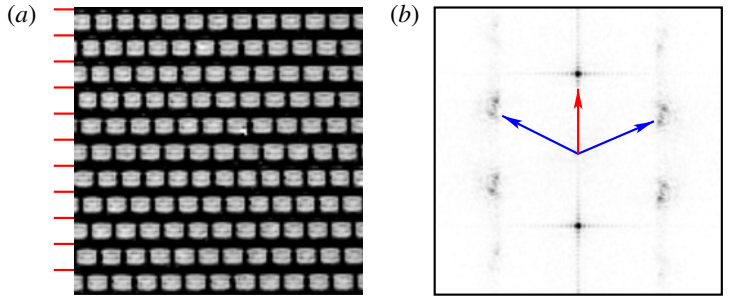


FIGURE 9. (Colour online) (*a*) Brickwall (BW) pattern taken at $q_f/q_c = 0.742$ and $\varepsilon = 0.289$. The lines at the left mark the forcing structure. (*b*) The centre part of its corresponding Fourier transform: the vertical arrow (red online) marks $\boldsymbol{q}_f$, and the angled arrows (blue online) are $\boldsymbol{q}_1$ and $\boldsymbol{q}_2$.

The three modes construct a resonant triad such that $\boldsymbol{q}_f = \boldsymbol{q}_1 + \boldsymbol{q}_2$. As a result, the amplitudes of these modes are coupled, quadratic terms appear in their corresponding amplitude equations and the up/down symmetry of the pattern is broken. That means, in our specific case, that there is no symmetry of the flow field in the z direction. As already briefly mentioned above, there are two reasons for the broken inverse symmetry. First, only the bottom plate is structured and not the top, and therefore the z-symmetry is already broken in the experiment. This has only a minor influence on the pattern for large q_f/q_c, since then the cell height d is large and therefore the forcing strength δ_f is small. With decreasing q_f/q_c, however, δ_f increases and this asymmetry between top and bottom becomes more pronounced. In addition, the critical temperature difference ΔT_c at which convection sets in the unforced

https://doi.org/10.1017/jfm.2014.456 Published online by Cambridge University Press

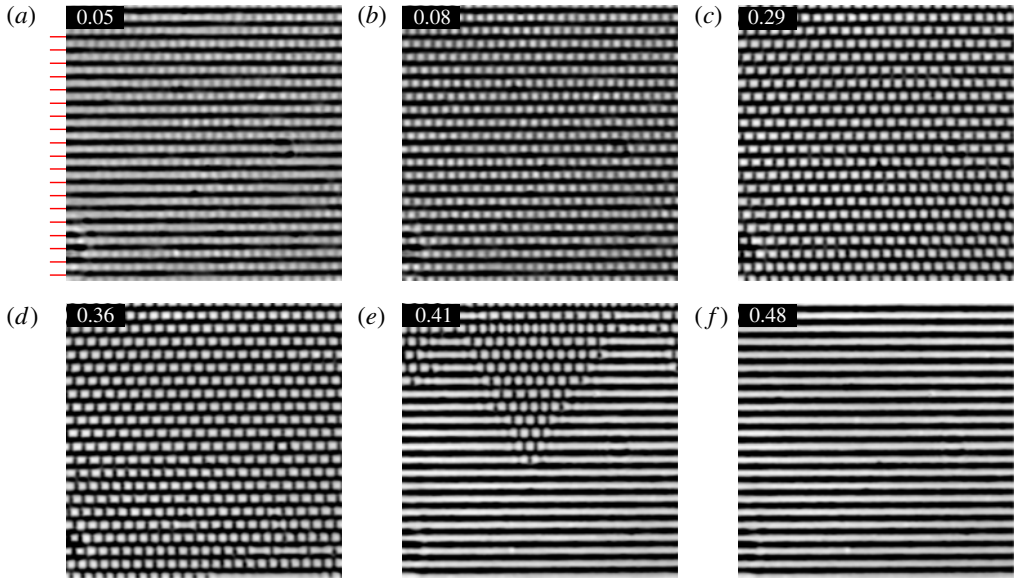


FIGURE 10. (Colour online) Development of BW pattern at $q_f/q_c = 0.74$ and various ε as marked on each image. Straight rolls became unstable at $\varepsilon = 0.05$ and turned into a BW pattern. When ε exceeded 0.48, straight rolls reoccurred. The lines at the left of the first image mark the location of the SU-8 ridges.

reference cell increases with decreasing q_f/q_c. Thus, the system becomes more non-Boussinesq, i.e. certain fluid properties (α, ν, κ) vary over the cell height. The cell height corresponding to the experiments in which the BW pattern was observed was $d \approx 340$–400 μm and the corresponding ΔT_c was ≈5 K. In this context it is also important to note that hexagons were observed in the reference cell for $q_f/q_c = 0.68$ ($d = 340$ μm). These hexagons did not cover the whole cell, but appeared at domain boundaries of rolls with different orientations.

As shown in figure 3, the theoretically predicted stability region of straight rolls strongly resembles the shape of the Busse balloon for the unforced RBC (figure 1). Specifically, the stability region is not symmetric with respect to q but leans to the left, i.e. to smaller values of q. With respect to the stability region of the forced system, this means that there is a range of q_f/q_c (for $q_f/q_c < 1$) in which straight rolls are stable for $\varepsilon < 0$, become unstable when ε is increased above zero and regain stability for $\varepsilon > \varepsilon_{c2}$, where the exact value of ε_{c2} depends on the applied q_f/q_c. In this range of q_f/q_c the maximal ε that could be reached experimentally was rather small due to the small d and corresponding large ΔT_c. However, with $q_f/q_c = 0.74$ we have at least one point where we could increase ε beyond ε_{c2} so that the system clearly re-enters the stability region of straight rolls (see figure 3). Figure 10 shows the evolution of BW pattern at $q_f/q_c = 0.74$ when ε is increased. For $\varepsilon = 0.05$ the straight rolls become unstable and a BW pattern occurs. A further increase of ε does not lead to additional modes and/or dynamical patterns, but results in the recurrence of stable rolls with wavevector $\boldsymbol{q}_f$ at $\varepsilon \approx 0.45$.

Even though we only have a single point, q_f/q_c, for the lower stability boundary of the straight roll stability region, our results confirm on the one hand qualitatively the theoretical predictions (Freund *et al.* 2011) regarding the shape of that region but on the other hand disagree quantitatively, as already mentioned above.

https://doi.org/10.1017/jfm.2014.456 Published online by Cambridge University Press

4. Summary and discussion

In this paper we have investigated experimentally the stability of convection rolls in a Rayleigh–Bénard system that was forced by a quasi-one-dimensional periodic modulation of the bottom plate profile. By varying the temperature difference ΔT and the cell height d in the experiment, we could change the dimensionless parameters ε and q_f and explore in detail the stability of straight rolls in the q_f/q_c–ε phase space.

Depending on the forcing wavenumber, straight rolls became unstable either to a varicose pattern (for $1.00 \lesssim q_f/q_c \lesssim 1.13$), or to kink defects ($1.19 \lesssim q_f/q_c \lesssim 1.30$), or to cross-rolls ($1.32 \lesssim q_f/q_c \lesssim 1.4$) or to a brickwall pattern ($0.63 \lesssim q_f/q_c \lesssim 0.74$).

As shown throughout this paper the shape of the stability region of straight rolls in the q_f/q_c–ε phase space agrees qualitatively with the theoretical predictions by Freund *et al.* (2011), but disagrees quantitatively. In the range $1 \leqslant q_f/q_c \leqslant 1.3$ the values of ε at which straight rolls become unstable are significantly larger in our experiment than predicted by theory. Furthermore, it was predicted that the instability has a very small Floquet vector $\boldsymbol{s}$ that decreases with decreasing δ_f and becomes zero for $\delta_f \to 0$ (skewed varicose instability). Here instead, we observed VP that consist of modes with a longer instability wavevector, that even increases when δ_f is reduced (q_f/q_c is increased). Solely in the range $1.19 \leqslant q_f/q_c \leqslant 1.3$ do straight rolls become unstable towards kinks that consist of a long-wavelength instability similar to SV instability in the unforced system.

Furthermore, in the range of $q_f/q_c > 1.25$ the theory (Freund *et al.* 2011) predicts oblique rolls for $\varepsilon > 0$. The experiments show instead CR with a single mode perpendicular to $\boldsymbol{q}_f$. For $q_f/q_c < 0.75$ we observed a BW pattern instead of oblique rolls as predicted by the theory.

Possible sources of discrepancy between the experimental observations and the theoretical predictions include the model assumptions concerning the applied forcing, the deviation in the experiments from the Oberbeck–Boussinesq regime and experimental imperfections and measurement uncertainties. With respect to the former, it should be noted that it has been assumed that a sinusoidal profile of the boundary can be treated theoretically as a flat boundary with a sinusoidal temperature modulation (McCoy 2007). Therefore, the forcing in Freund *et al.* (2011) was introduced by a sinusoidal temperature modulation of the bottom plate. However, in our experiments the bottom plate has a step-like forcing pattern instead of a sinusoidal one. In addition, both the temperature and the velocity field are modulated at the bottom plate. By mapping only the surface modulation onto a temperature modulation, one neglects an additional contribution from the modulated temperature field. This would explain in particular the higher stability line for straight rolls in the experiment for the range $q_f/q_c \geqslant 1$. But it could also be a possible explanation for the different patterns observed. We have observed CR, where actually oblique rolls were expected (for $q_f/q_c > 1.32$). In fact, the instability lines for CR and oblique rolls are very close to each other. Therefore, CR might also be observed in a theory if better matching boundary conditions were incorporated.

With respect to the deviation from the Oberbeck–Boussinesq condition, we note that, especially on the left-hand side of the stability region, the cell height was small, and thus δ_f and ΔT_c were large. Both effects are breaking the up-down symmetry ('Boussinesq symmetry'). While this symmetry was also broken in the theoretical description, the effect there was only weak, since only the temperature at the bottom plate was modulated with a small δ_f, whereas otherwise full Oberbeck–Boussinesq conditions were assumed. The BW patterns we have observed, for instance, are clearly not symmetric with respect to inversion of the warm and cold

https://doi.org/10.1017/jfm.2014.456 Published online by Cambridge University Press

areas (up- and down-flow areas) and are most likely caused by the strong deviation from the symmetric system.

Finally, it is interesting, that a simple shift of the q_f/q_c-axis in figure 3 would result in a much better agreement. Such a shift could be caused, for example, by a systematic error of either the forcing wavelength ($2\pi/q_f$), or the cell height ($3.117/q_c$). Since the periodicity of the SU-8 ridges of the bottom plate was measured with high accuracy, it is more likely that there is a systematic error in the cell height d. We can easily estimate what the error in d must be, in order to explain the shift in q_f/q_c. Looking at the bottom of the wedge-shaped region in figure 3, we estimate a shift of $\Delta(q_f/q_c) \approx 0.15 = \Delta_s 2\pi/3.117$, where Δ_s denotes a systematic error in the cell height. Solving this equation reveals $\Delta_s \approx 74$ μm. Surprisingly, this value is close to the height of our SU-8 ridges ($h = (65 \pm 3)$ μm). While this result suggests, that the systems behaves as if the cell height were reduced by the height of the ridges (h), this might also be just a coincidence since only a tenth of the area is covered with ridges and thus the average height is expected to be reduced by only $h/10$.

Is it possible, that we have systematically overestimated the cell height? We determined the cell height via the critical temperature difference ΔT_c at which convection sets in for the unforced reference cell. While ΔT is measured with high precision, the instability in the unforced reference cell can occur at slightly smaller ΔT_c than in an infinitely extended system, due to the rather small aspect ratio (see e.g. Stork & Müller 1975; Brown & Stewartson 1978; Cross & Hohenberg 1993). This would lead to an overestimation of the cell height and of q_f/q_c. This effect would be significantly larger on the right-hand side of the phase diagram, since there, the aspect ratio is smaller and thus the influence of the sidewall forcing larger. Based on the shadowgraph images we can roughly estimate the influence of the sidewall forcing and thus the uncertainty of ΔT_c. Even for the largest cell height of $d = 690$ μm (smallest aspect ratio of the unforced reference cell), we expect the error of ΔT_c to be smaller than 5 %. An underestimation of ΔT_c of 5 %, would lead to an overestimation of d of less than 2 %. However, we would have to explain an error in the cell height of 10 % to match experiment and simulations. Thus, we can state that sidewall forcing can account at most only for a small amount of the shift necessary to match experiment and theory.

Acknowledgements

We highly acknowledge Professor W. Pesch for providing us the software to calculate the stability of straight rolls for the forced and the unforced system. We further thank him for fruitful discussions and constructive advices.

REFERENCES

BERRY, M. V. & BODENSCHATZ, E. 1999 Caustics, multiply reconstructed by talbot interference. *J. Mod. Opt.* **46** (2), 349–365.

BODENSCHATZ, E., PESCH, W. & AHLERS, G. 2000 Recent developments in Rayleigh–Bénard convection. *Annu. Rev. Fluid Mech.* **32**, 709–778.

BOUSSINESQ, J. 1903 *Theorie Analytique de la Chaleur,* vol. 2. Gauthier-Villars.

BROWN, S. N. & STEWARTSON, K. 1978 On finite amplitude Benard convection in a cylindrical container. *Proc. R. Soc. Lond.* A **360** (1703), 455–469.

DE BRUYN, J. R., BODENSCHATZ, E., MORRIS, S. W., TRAINOFF, S., HU, Y., CANNELL, D. S. & AHLERS, G. 1996 Apparatus for the study of Rayleigh–Bénard convection in gases under pressure. *Rev. Sci. Instrum.* **67**, 2043–2067.

https://doi.org/10.1017/jfm.2014.456 Published online by Cambridge University Press

BUSSE, F. H. 1967 The stability of finite amplitude cellular convection and its relation to an extremum principle. *J. Fluid Mech.* **30**, 625–649.

BUSSE, F. H. 1978 Nonlinear properties of convection. *Rep. Prog. Phys.* **41**, 1926–1967.

BUSSE, F. H. & WHITEHEAD, J. A. 1971 Instabilities of convection rolls in a high Prandtl number fluid. *J. Fluid Mech.* **47**, 305–320.

BUSSE, F. H. & WHITEHEAD, J. A. 1974 Oscillatory instabilities in large Prandtl number convection. *J. Fluid Mech.* **66**, 67–79.

CHEN, M. M. & WHITEHEAD, J. A. 1968 Evolution of two-dimensional periodic Rayleigh convection cells of arbitrary wavenumbers. *J. Fluid Mech.* **31**, 1–15.

CROSS, M. & GREENSIDE, H. 2009 *Pattern Formation and Dynamics in Nonequilibrium Systems*. Cambridge University Press.

CROSS, M. C. & HOHENBERG, P. C. 1993 Pattern formation outside equilibrium. *Rev. Mod. Phys.* **65** (3), 851.

FREUND, G., PESCH, W. & ZIMMERMANN, W. 2011 Rayleigh–Bénard convection in the presence of spatial temperature modulations. *J. Fluid Mech.* **673**, 318–348.

HOYLE, R. 2006 *Pattern Formation – An Introduction to Methods*. Cambridge University Press.

KELLY, R. E. & PAL, D. 1978 Thermal convection with spatially periodic boundary conditions: resonant wavelength excitation. *J. Fluid Mech.* **86**, 433–456.

KESSLER, M. A. & WERNER, B. T. 2003 Self-organization of sorted patterned ground. *Science* **299**, 380–383.

KLAUSMEIER, C. A. 1999 Regular and irregular patterns in semiarid vegetation. *Science* **284**, 1826–1828.

KUECKEN, M. & NEWELL, A. C. 2005 Fingerprint formation. *J. Theor. Biol.* **235**, 71–83.

LOWE, M. & GOLLUB, J. P. 1985 Solitons and the commensurate–incommensurate transition in a convecting nematic fluid. *Phys. Rev.* A **31** (6), 3893–3897.

LOWE, M., GOLLUB, J. P. & LUBENSKY, T. C. 1983 Commensurate and incommensurate structures in a non-equilibrium system. *Phys. Rev. Lett.* **51** (9), 786–789.

LUTHER, S., FENTON, F. H., KORNREICH, B. G., SQUIRES, A., BITTIHN, P., HORNUNG, D., ZABEL, M., FLANDERS, J., GLADULI, A., CAMPOY, L., CHERRY, E. M., LUTHER, G., HASENFUSS, G., KRINSKY, V. I., PUMIR, A., GILMOUR, R. F. JR & BODENSCHATZ, E. 2011 Low-energy control of electrical turbulence in the heart. *Nature* **475**, 235–239.

MANOR, R., HAGBERG, A. & MERON, E. 2008 Wavenumber locking in spatially forced pattern-forming systems. *Europhys. Lett.* **83**, 10005 (p. 1–6).

MARTIN, C. P., BLUNT, M. O., PAULIAC-VAUJOUR, E., STANNARD, A., MORIARTY, P., VANCEA, I. & THIELE, U. 2007 Controlling pattern formation in nanoparticle assemblies via directed solvent dewetting. *Phys. Rev. Lett.* **99** (11), 116103.

MAU, Y., HAIM, L., HAGBERG, A. & MERON, E. 2013 Competing resonances in spatially forced pattern-forming systems. *Phys. Rev.* E **88**, 032917.

MCCOY, J. H. 2007 Adventures in pattern formation: spatially periodic forcing and self-organization. PhD thesis, Cornell University.

MCCOY, J. H., BRUNNER, W., PESCH, W. & BODENSCHATZ, E. 2008 Self-organization of topological defects due to applied constraints. *Phys. Rev. Lett.* **101** (25), 254102.

MURRAY, J. D. 1989 *Mathematical Biology*. Springer.

OBERBECK, A. 1879 Über die Wärmeleitung der Flüssigkeiten bei Berücksichtigung der Strömungen infolge von Temperaturdifferenzen. *Ann. Phys. Chem.* **7**, 271–292.

PLAPP, B. B. 1997 Spiral pattern formation in Rayleigh–Bénard convection. PhD thesis, Cornell University.

PORTER, J. & SILBER, M. 2004 Resonant triad dynamics in weakly damped faraday waves with two-frequency forcing. *Physica* D **190** (1–2), 93–114.

RASENAT, S., HARTUNG, G., WINKLER, B. L. & REHBERG, I. 1988 The shadowgraph method in convection experiments. *Exp. Fluids* **7**, 412–420.

ROGERS, J. L., SCHATZ, M. F., BRAUSCH, O. & PESCH, W. 2000 Superlattice patterns in vertically oscillated Rayleigh–Bénard convection. *Phys. Rev. Lett.* **85** (20), 4281–4284.

https://doi.org/10.1017/jfm.2014.456 Published online by Cambridge University Press

SEIDEN, G., WEISS, S., MCCOY, J., PESCH, W. & BODENSCHATZ, E. 2008 Pattern forming system in the presence of different symmetry-breaking mechanisms. *Phys. Rev. Lett.* **101**, 214503.

SPIEGEL, E. A. & VERONIS, G. 1960 On the Boussinesq approximation for a compressible fluid. *Astrophys. J.* **131**, 442–447.

STORK, K. & MÜLLER, U. 1975 Convection in boxes: an experimental investigation in vertical cylinders and annuli. *J. Fluid Mech.* **71**, 231–240.

TABERLET, N., MORRIS, S. W. & MCELWAINE, J. N. 2007 Washboard road: the dynamics of granular ripples formed by rolling wheels. *Phys. Rev. Lett.* **99**, 068003.

TIAN, W., PARKER, D. J. & KILBURN, C. A. D. 2003 Observation and numerical simulation of atmospheric cellular convection over mesoscale topography. *Mon. Weath. Rev.* **131**, 222–235.

TRAINOFF, S. P. & CANNELL, D. S. 2002 Physical optics treatment of the shadowgraph. *Phys. Fluids* **14**, 1340–1363.

TSCHAMMER, A. 1996 Nichtlineare Aspekte der Rayleigh–Bénard Konvektion in isotropen und anisotropen Fluiden. PhD thesis, Universität Bayreuth.

TURING, A. M. 1952 The chemical basis of morphogenesis. *Phil. Trans. R. Soc. Lond.* B **237** (641), 37–72.

WEISS, S. 2009 Pattern formation in spatially forced thermal convection. PhD thesis, Georg-August-Universität Göttingen.

WEISS, S., SEIDEN, G. & BODENSCHATZ, E. 2012 Pattern formation in spatially forced thermal convection. *New J. Phys.* **14**, 053010.

https://doi.org/10.1017/jfm.2014.456 Published online by Cambridge University Press